

# Landslide hazard zonation in high risk areas of Rethymno Prefecture, Crete Island, Greece

Maria Kouli · Constantinos Loupasakis · Pantelis Soupios ·  
Filippos Vallianatos

Received: 18 June 2008 / Accepted: 20 April 2009 / Published online: 8 May 2009  
© Springer Science+Business Media B.V. 2009

**Abstract** The central part of Rethymnon Prefecture, Crete Island, suffers from severe landslide phenomena because of its geological and geomorphological settings alternated by the human activities. The main landslide preparatory and triggering causal factors are considered to be the ground conditions (lithology), geomorphological processes (fluvial erosion, etc.), and the man-made actions (excavations, loading etc.). The purpose of this study is to develop a decision support and continuous monitoring system of the area by composing landslide hazard and risk maps. For that reason, several approaches of the weighted linear combination (WLC), a semi-quantitative hazard analysis method, were adopted in a Geographic Information Systems (GIS) environment. The results were validated using a pre-existing landslide database enriched with new landslide locations mapped through image interpretation of a processed IKONOS satellite image. The validation results showed that the WLC method coupled with remote sensing (RS) and GIS techniques can support engineering geological studies concerning landslide vulnerability of hazardous areas.

**Keywords** Landslide hazard zonation · GIS · Satellite images · Rethymnon area · Crete Island

## 1 Introduction

Landslides are considered to be one of the most dangerous natural hazards due to the fact that they cause human casualties and extensive damages worldwide. A landslide hazard map depicts areas prone to landslides by integrating the causal and triggering factors of the

---

M. Kouli (✉) · P. Soupios · F. Vallianatos  
Institute of Natural Resources and Natural Hazards, Center of Technological Research of Crete (CTRC), 3 Romanou, Chalepa, 73133 Chania, Crete Island, Greece  
e-mail: mkouli@chania.teicrete.gr

C. Loupasakis  
Engineering Geology Department, Institute of Geology and Mineral Exploration (IGME), Olympic Village, Thracomacedones, 13677 Athens, Greece

landslides with data concerning the past distribution of slope failures (Brabb 1984; Fall et al. 2006). Crucial factors for the construction of reliable hazard maps are the quality and the amount of available data and the selection of the best method for the analysis.

There are three main landslide risk assessment approaches and these are qualitative, semi-quantitative, and quantitative (Lee and Jones 2004; Castellanos Abella and van Westen 2008). Quantitative methods are based on mathematical expressions of the correlation between causal factors and landslides. The two types of quantitative methods that are commonly used are deterministic and statistical (Ward et al. 1981; Nash 1987; Terlien et al. 1995; Atkinson and Massari 1998; Aleotti and Chowdhury 1999; Fall and Azzam 2001a, b). The quantitative assessments involve analytic bivariate, multivariate, logistics regression, fuzzy logic, artificial neural network analysis, etc. (Carrara et al. 1995; van Westen et al. 1997; Aleotti and Chowdhury 1999; Dai et al. 2002; Ercanoglu and Gokceoglu 2004; Lee et al. 2004a, b; Komac 2006; Caniani et al. 2008).

On the other hand, qualitative methods are based on expert opinions (Nash 1987; Anbalagan 1992; Fall et al. 1996; Evans et al. 1997; Leroi 1997; Atkinson and Massari 1998; Guzetti et al. 1999; Fall et al. 2006). The basic types of qualitative methods use landslide index to identify areas with similar geological and geomorphologic characteristics that are susceptible to landslides. Moreover, there are qualitative methodologies which use weighting and rating procedures and these are known as semi-quantitative methods (Hutchinson and Chandler 1991; Siddle et al. 1991; Moon et al. 1992; Fell et al. 1996; Ayalew and Yamagishi 2005). Such kinds of methodologies are the analytic hierarchy process (AHP) (Saaty 1980; Barredo et al. 2000; Yalcin 2008) and the weighted linear combination (WLC) (Ayalew et al. 2004a, b; Ayalew and Yamagishi 2005). The AHP methodology involves the creation of hierarchy of decision elements (factors) and the comparison between different pairs of elements in order to assign a weight and a consistency ratio for each element.

The WLC approach involves the combination of several landslide parameters' maps. In each class of the map—thematic layer in the sense of GIS—a corresponding rating value is assigned and then the parameter layers are weighted according to the importance or preference of each parameter relative to the others. Finally, all the derived maps are overlaid in order to construct the final landslide hazard map. Although the results of these approaches are partly subjective depending on the knowledge of experts (van Westen et al. 1997; Leroi 1997; Fall 2000; Fall et al. 2006), the qualitative or semi-quantitative methods have been proved to be notably useful in the case of regional studies (Soeters and van Westen 1996; Guzetti et al. 1999; Ayalew et al. 2004b).

According to De Roo (1993), Geographic Information Systems (GIS) is a tool for collecting, storing, retrieving, transforming, manipulating, and displaying spatially distributed data, and therefore it is frequently used in distributed deterministic modeling. In nowadays, the development of GIS has enhanced the capabilities for the research of landslides susceptibility (Carrara et al. 1995; Dikau et al. 1996; Carrara et al. 1999; Miles and Ho 1999; Miles and Keefer 1999; Luzi et al. 2000; Fall 2000; Refice and Capolongo 2002; Fall et al. 2006) while many studies have been carried out to overview the use of GIS for landslide susceptibility assessment (van Westen 1994; Carrara et al. 1995; Aleotti and Chowdhury 1999; Dai et al. 2002; Cevik and Topal 2003; Ayalew and Yamagishi 2005; Fall et al. 2006). Moreover, remote sensing (RS) techniques are widely used in landslide susceptibility assessment in both the generation of landslide parameters thematic layers and the production of landslide inventory maps (Saha et al. 2002; Park and Chi 2007).

In this study, the ordinal scale (qualitative) hazard analysis using relative weighting-rating system has been adopted for landslide hazard zonation. The goal of the present study is the implementation of the WLC method in an area which suffers from severe landslide

phenomena, situated within the geographic limits of Rethymno Prefecture in Crete Island. The applicability and the efficiency of GIS and RS methods for landslide hazard zonation are also presented.

## 2 Geological framework

Crete Island is characterized by an extremely complicated geological structure with intensive tectonic fragmentation. Although many researchers through the years have studied the geological evolution of the island (Tataris and Christodoulou 1965; Bonneau 1973; Creutzburg 1977; Fitroulakis 1980; Tsiampaos 1989), there are still many unsolved issues. Based on current theories, the island constitutes of repeated tectonic covers consisting of variant geotectonic zones' geological series.

The study area is situated in the central to southern part of Rethymnon Prefecture. The total area is 81.5 km<sup>2</sup> and is geographically defined from the Patsos village to the west, the Pantanassa village to the north, the Fourfouras village to the east and the Vrysses village to the south encompassing numerous other villages (Fig. 1). According to the landslide hazard zonation map of Greece (Koukis et al. 2005), the broader area located in the central part of Rethymnon Prefecture exhibits the highest frequency of landslides occurrences in the island of Crete (Fig. 2).

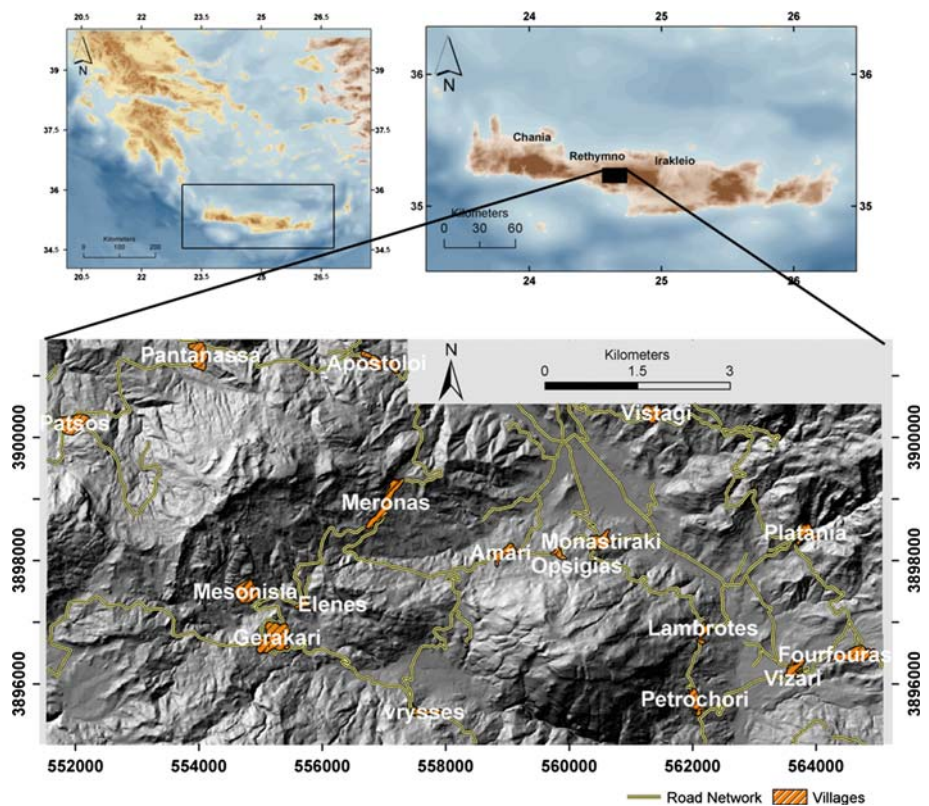


**Fig. 1** Location maps and the digital elevation model of the area under investigation

**Fig. 2** Landslide hazard zonation map of Greece showing the number of landslides per 100 km<sup>2</sup> (Koukis et al. 2005)

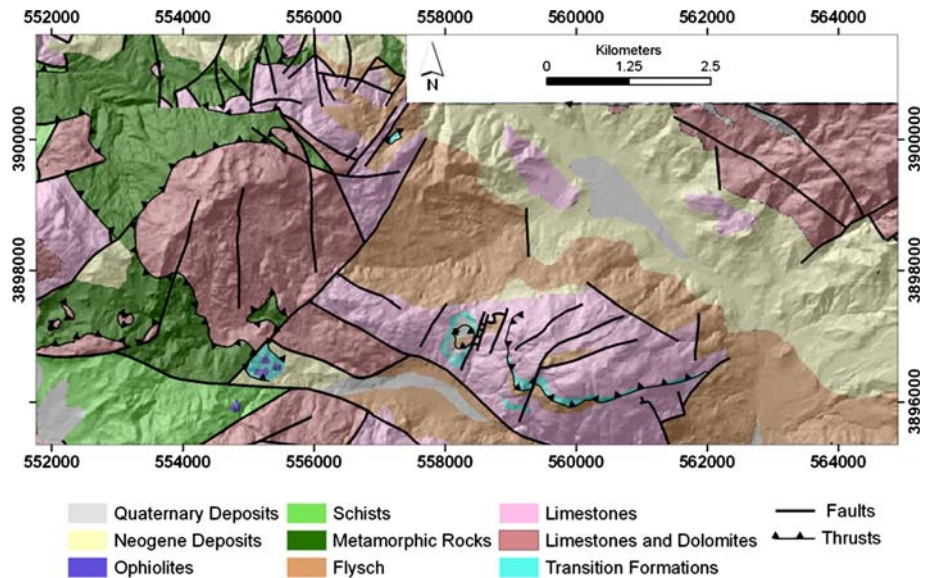
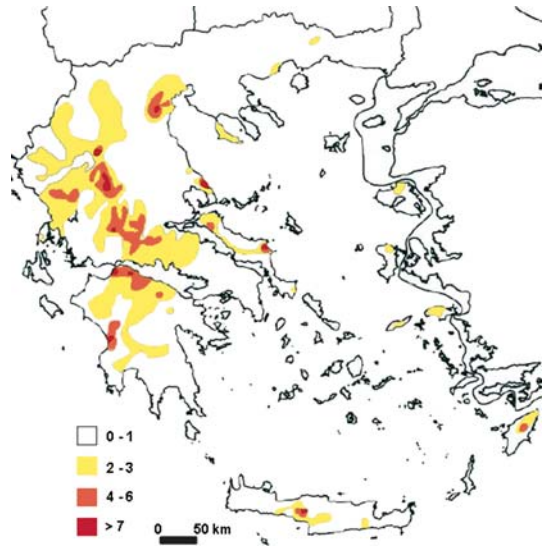


**Fig. 3** Geological map of the study area superimposed to the Digital Elevation Model (DEM) of the study area (IGME 1985, 1991)

As presented in the unified geological map of (Fig. 3), the study area is occupied by: (1) loose Quaternary deposits (alluvial deposits, slope debris and fans, and torrent terraces), (2) Neogene deposits (limestones, conglomerates, sandstones, and clays), (3) tectonic covers of Pindos and Tripolis geotectonic zones consisting of limestones and marbles (plattenkalk, dolomites, and undivided carbonated formations), flysch and metamorphic rocks (phyllites, quartzites, shales, schists, and meta-sandstones), and (4) ophiolites of the autochthonous Ionian zone.

**Table 1** Frequency and relative frequency distribution of landslides in Greece, in relation to the lithological type (Koukis et al. 1994, 2005) compared with the extend of the lithological types in the study area

Lithological type	Frequency of landslides (%)	Relative frequency of landslides (%)	Extend (%) of the lithological types in the study area
Loose Quaternary deposits	20.65	12.99	15.87
Neogene	28.20	11.74	24.00
Flysch	30.35	35.75	8.48
Schist-cherts	3.62	29.64	1.22
Limestones, marbles	4.85	2.48	19.50
Metamorphic	9.32	5.07	18.35
Volcanic	3.00	2.37	12.58

The area under investigation presents favorable conditions for landslide activity. Considering the fact that the 20% of the area is occupied by flysch and the 22% by loose Quaternary deposits and Neogene, the frequency of the landslides can be expected to be very high. As presented in Table 1 (Koukis et al. 1994, 2005), these formations are related with the 80% of the landslides occurred in Greece. Based on in-situ observations, beside the previously mentioned formations, within the limits of the study area, many landslides occur in sections occupied by the weathered mantle of the metamorphic rocks and by the calcitic rock formations.

The extensive tectonic fragmentation and the repeated thrusts, the intense morphological relief with the steep slopes, the dense drainage network with the deep valleys, the extensive human activities with the relatively dense road network, and the arable-irrigated areas are some of the preparatory and triggering causal factors of the landslides in the study area besides the type of the geological formations.

The majority of the landslides occurring in loose Quaternary deposits, Neogene sediments, and weathered mantle of metamorphic rocks or flysch are translational—rotational slides (Fig. 4a) (Varnes 1978). The extension of the sliding area depends on the geometry of the slope and in some cases they affected areas reaching up to 0.5 Km<sup>2</sup> (e.g., rotational slide in Quaternary deposits along the Akoumia–Kria Vrissi road axis in the wider study area). Moreover, creep movements are recorded on areas covered by loose formations or by weathered mantles of metamorphic rocks or flysch. This kind of movements, in some cases, it was recorded that they affected entire villages causing extended damages. Two characteristic examples, villages damaged by creep movements are Pantanasa and Apostoli founded on the weathered mantles of metamorphic rocks (Fig. 4b, d).

On areas occupied by rock formations (e.g., marbles and limestones) with very steep slopes, extensive debris flow are recorded (Fig. 4c). Planar slides or wedge failures also occur in these formations but they can be characterized as failures of local importance.

### 3 Data used and methodology

The different types of datasets used for the landslide hazard zonation of the area under investigation were as follows:

1. Geological maps of the Institute of Geology and Mineral Exploration representing lithological and structural units at 1:50000 scale (IGME 1985, 1991).

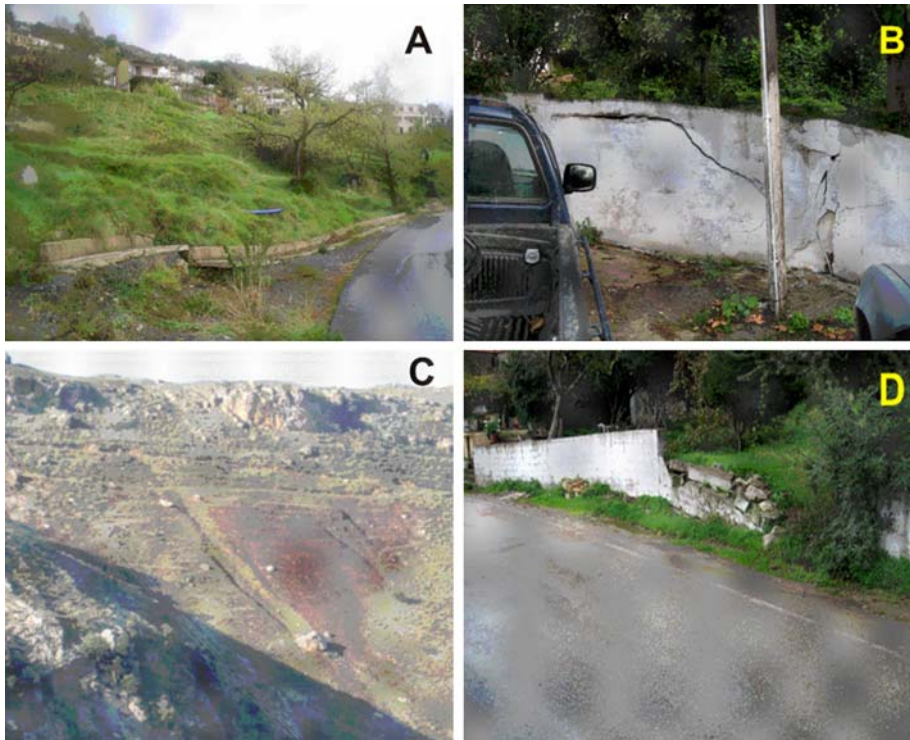


**Fig. 4** **a** Rotational slide south to Merona occurred in the weathered mantle of Flysch formations. This landslide damaged an overloaded slope under excavated during the construction of the road. **b** Damages on a fencing caused by the creep sliding in Pantanasa village. **c** Debris flow originating from a very steep limestone slope. **d** Damages on a fencing caused by the creep sliding in Apostoli village

2. Topographic maps of the Hellenic Military Geographical Service at a scale of 1:5000 to form a detailed base map with 4-m contour interval.
3. Satellite sensor data and in particular, an IKONOS-2 image acquired on 2006-07-27 with a spatial resolution of 4 m for the multi-spectral bands (4 bands) and 1 m for the panchromatic image.
4. The Corine Land Cover map 2000 (CLC2000 100 m, version 1) of the European Environment Agency (©EEA, Copenhagen, 2000; <http://www.eea.europa.eu>). This map has a resolution of 100 m and uses 10 land use categories for the study area from a total of 44 land uses of level 3.
5. Precipitation data covering a time period of 25 years.
6. Field data involving observations on geology, tectonic structures, and recorded landslide occurrences.

In order to create the appropriate information platform upon which to proceed in a systematic way toward applying the landslide models, all available data in the form of maps were used as the basis for the creation of GIS thematic layers.

The data pre-processing involved in their implementation into ArcGIS Desktop 9.1 software environment. The several maps were geo-referenced to the local projection system of Greece (GGRS '87—Greek Geodetic Reference System), so that they could all be tied to the same projection system, together with all future information that may become

available. In the next pre-processing phase, digitization of all the relevant data maps, namely lithological, structural and topographical was carried out. The Digital Elevation Model (DEM) of the study area with a cell size of 4 m is a continuous raster layer, in which data values represent elevation. The DEM was generated from the topographic maps of the study area. Many terrain attributes such as slope gradient, aspect, relative relief, and stream network were derived from further processing of the DEM (Fig. 5).

### 3.1 Satellite image processing

In the last years, available high-resolution data (e.g., a pixel resolution of 1 m or less) such as IKONOS and QuickBird imagery are used to detect small-scale landslides. The IKONOS-2 satellite image acquired on 27th of July 2006 is cloud free with no visible signs of localized haze. The above mentioned product was supplied in the “standard geometrically corrected” level using the cubic convolution interpolation method. This product is not corrected for terrain distortions. In order to remove the topography-related distortions caused by terrain relief, an ortho-photo was generated using the rational polynomial coefficient (RPC) model and a high-resolution DEM of 4-m cell size, in ERDAS Imagine 9.0 software environment. The RPC model uses ratios of cubic polynomials to express the transformation from ground surface coordinates to image coordinates. The coefficients for the rational polynomial model are supplied in an auxiliary text file linked with the IKONOS image. The final image was created using a pan-sharpening technique that combines the 1-m spatial resolution of the panchromatic image with the high spectral resolution of the 4-m spatial resolution multi-spectral image (four bands: blue, green, red, and near infrared). Principal Component Analysis (PCA) was applied to the pan-sharpened satellite image. The principal component analysis minimizes the number of linear combinations from the original data retaining as maximum information as possible. The three-first principal components were automatically computed. The second principal component (PC2) was used for the extraction of the road network of the study area using on-screen digitization while at the same time, the photo-interpretation of the third principal component (PC3) helped to discriminate paved from unpaved roads and as a result many footpaths of no interest for the current study were excluded of the road network layer (Fig. 6).

Furthermore, the IKONOS pan-sharpened image with a final spatial resolution of 1 m was used for the correction and update of the land use map, while using several color composites, several probable landslide occurrences were mapped, contributing to the verification of the landslide hazard maps.

### 3.2 Data layer preparation

After the creation of the primary layers, namely lithology, tectonic structures, land use, road network, stream network, and Digital Elevation Model, various advanced GIS techniques, such as filtering, distance buffering, logical operations, vector to raster conversion, reclassification, and raster calculations were applied.

For the landslide hazard zonation, which was the aim of this study, the following data layers (Fig. 5) were finally prepared and used.

#### 3.2.1 Lithology map

The landslide phenomenon is closely related to the lithology and weathering properties of the materials. In the area under investigation, the rock outcrops are decomposed at different

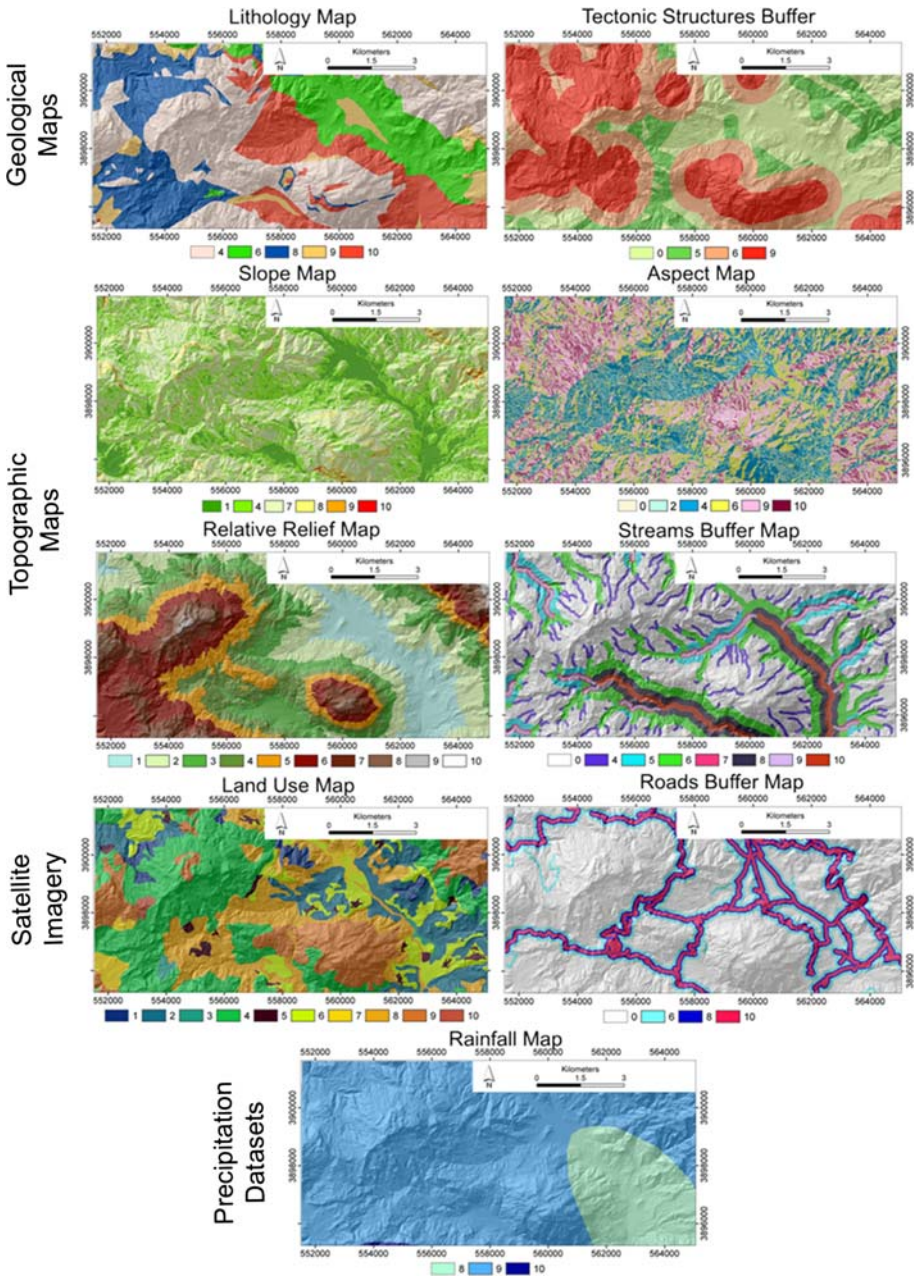


**Fig. 5** The final rated data layers which were used as input parameters for the raster calculator overlay function

degrees. The lithology layer has been derived through the digitization of the published geological maps (IGME 1985, 1991) which display major rock groups and structural features. The lithological formations (Fig. 3) were classified into five broad categories



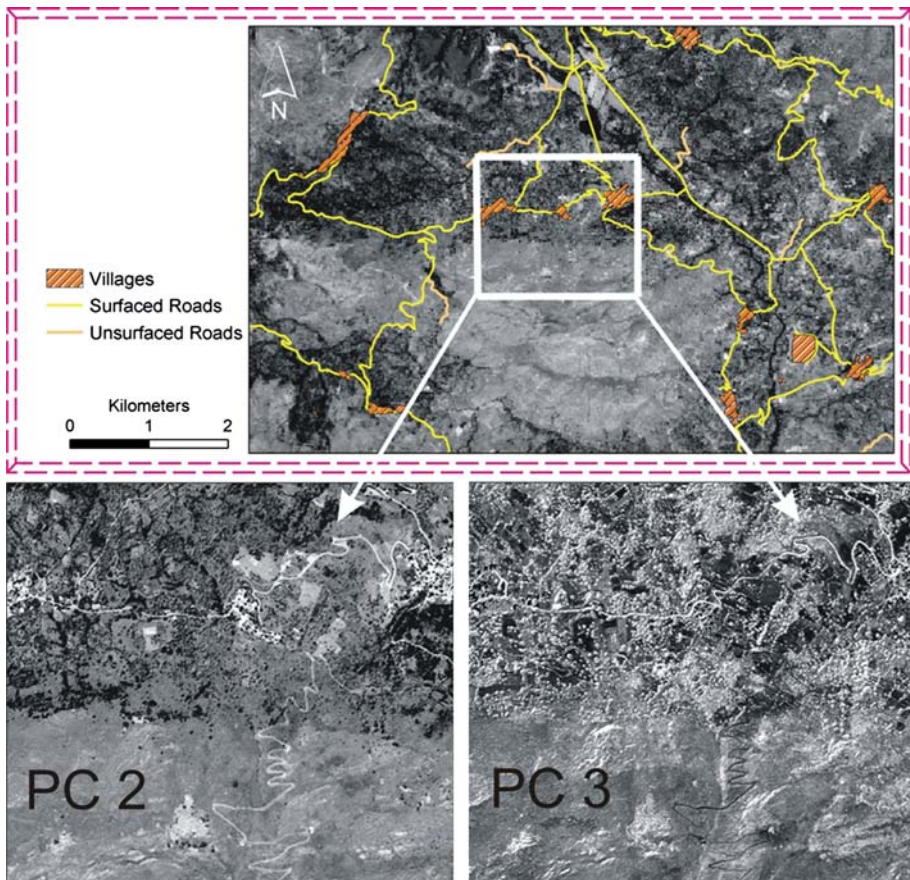


**Fig. 6** Second principal component (PC2) with superimposed the extracted road network. The lower figures show part of the road network on PC2 and PC3 images (note the difference of the curved road in the center of the images which was finally interpreted as footpath)

based on landslide susceptibility (Table 2): (a) limestones and marbles, (b) neogene sediments, (c) schists and ophiolites, (d) loose Quaternary deposits, and (e) flysch (Fig. 3).

### 3.2.2 Buffer map of tectonic structures

Tectonic structures, such as thrusts and faults, are usually associated with extensive fractured zones and steep relief anomalies. These zones present favorable conditions for landslides. Therefore, major structural discontinuities produced by faults and fractures were included as a parameter in this study.

A distance function was applied to create buffer zones, at a distance of 500 m around the fault/fracture lineament (250 m from either side), in order to produce two broad classes: ‘near’ or ‘distant’ (Table 2). Similarly, multiple buffer zones at distances of 0–500 and 500–1000 m around the thrusts were created, which producing three classes: “nearest”, “near,” and “distant” (Table 2).

**Table 2** Various data layers and landslide hazard weighting-rating system adopted in this study

Data layers	Classes	$W_1$	$W_2$	Rate
Lithology	Loose quaternary deposits (Alluvial deposits, slope debris and fans, torrent terraces)	10	10	9
	Neogene (reefal limestones, Pantanassa formation)			6
	Limestones–marbles (Platy limestones, limestones and dolomites, carbonate undivided layers)			4
	Flysch			10
	Schists and ophiolites (phyllites, quartzites, shales, schists)			8
	Tectonic structures	Thrust (Buffer)	9	0.9 * Lithology layer
<500 m				9
500–1000 m				6
>1000 m				0
Fault (Buffer)				
<250 m				5
	>250 m			0
Landuse	Sparsely vegetated areas	8	0.8 * Lithology layer	10
	Natural grasslands			9
	Land principally occupied by agriculture, with significant areas of natural vegetation			8
	Non-irrigated arable land			7
	Complex cultivation patterns			6
	Discontinuous urban fabric			5
	Sclerophyllous vegetation			4
	Vineyards			3
	Olive groves			2
	Coniferous forest—transitional woodland			1
Roads	Unsurfaced (Buffer)	7	0.7 * Lithology layer	
	<50 m			6
	>50 m			0
	Surfaced (Buffer)			
	<50 m			10
	50–100 m			8
	100–200 m			6
	>200 m			0
Streams	Class 1 (Buffer)	8	0.8 * Lithology layer	
	<50 m			4
	>50 m			0
	Class 2 (Buffer)			
	<100 m			6
	>100 m			0
	Class 3 (Buffer)			
	<50 m			9
	50–100 m			7

**Table 2** continued

Data layers	Classes	$W_1$	$W_2$	Rate
	100–300 m			5
	>300 m			0
	Class 4 (Buffer)			
	<100 m			10
	100–300 m			8
	300–600 m			6
	>600 m			0
Slope	>61°	9	0.9 * Lithology layer	10
	46–60°			9
	31–45°			8
	16–30°			7
	6–15°			4
	0–5°			1
Relative relief	1000–901 m	6	0.6 * Lithology layer	10
	900–801 m			9
	800–701 m			8
	700–601 m			7
	600–501 m			6
	500–401 m			5
	400–301 m			4
	300–201 m			3
	200–101 m			2
	100–0 m			1
Aspect	W, N	6	0.6 * Lithology layer	9
	NW			10
	NE, SW			6
	E, S			4
	SE			2
	Flat			0
Rainfall	1400–1200	8	0.8 * Lithology layer	10
	1200–1000			9
	1000–800			8

### 3.2.3 Landuse map

Landuse is also related with the triggering and causal factors of the landslides. For instance, some types of land use/cover, especially of woody vegetation with large and strong root systems, provide both hydrological and mechanical effects that generally stabilize slopes (Gray and Leiser 1982; Greenway 1987; Montgomery et al. 2000). On the contrary, landslides occur in unvegetated or irrigated cultivated areas due to the lack of the previously mentioned effects. Therefore, the role of vegetation in the slope stability was evaluated by using the updated, through the IKONOS pan-sharpened image, Corine Land Use 2000 map with 10 classes for the study area. The different land uses were ranked as shown in Table 2.

### 3.2.4 Buffer map of roads

Extensive excavations, application of external loads, and vegetation removal are some of the most common actions taking place along the road network slopes, during their construction. These attended actions are also responsible for the landslide triggering (WP/WLI 1994), and due to this reason, the road network and buffer zones along it must be evaluated during the analysis.

Using the second and the third Principal Component of the pan-sharpened IKONOS-2 satellite image, the road network vector layer was produced (Fig. 6). Two different kinds (attributes) of roads were used; unsurfaced and surfaced roads. A buffer zone of 50 m of either side of unsurfaced roads was applied, producing two classes (near and distant). Similarly, multiple buffer zones were applied to surfaced roads producing four classes (within a distance of 50, 50–100, 100–200, and >200 m) (Table 2).

### 3.2.5 Buffer map of streams

Fluvial erosion of slopes toe is one of the most common triggering casual factors of the landslides, especially in areas with the intense morphological relief and dense drainage network with the deep valleys. The distance from rivers is therefore considered as an important factor in characterizing susceptible areas.

The drainage network was automatically extracted from the DEM and the drainage tributaries were then classified according to Strahler's system (Strahler 1957, 1964).

A drainage buffer map was produced based on stream order. In this context, streams of the 1st order were buffered at a distance of 50 m, streams of 2nd order were buffered at a distance of 100 m, and streams of 3rd order were multiply buffered at distances of 50, 50–100, 100–300, and >300 m giving rise to four classes. Finally, the streams of 4th order were also multiply buffered at 100, 100–300, 300–600, and >600 m, (Table 2).

### 3.2.6 Slope angle map

Slope angle and geometry are controlling factors in slope stability (Huang and Li 1992; Wu et al. 2001), and a digital slope image is therefore a fundamental part of a hazard assessment model (Clerici et al. 2002; Saha et al. 2002; Cevik and Topal 2003; Ercanoglu and Gokceoglu 2004; Lee et al. 2004a, b; Yalcin 2008).

Slope angle was extracted from the DEM, using a  $3 \times 3$  kernel filter and the derived slope angle image has values ranging from 0 to  $68.6^\circ$  (Table 3). Geographically, steep slopes ( $>30^\circ$ ) are widespread, with extended 'flat' areas. The produced slope image was thresholded into six slope angle classes ('flat', 'gentle', "moderate", "moderately steep", 'steep,' and 'very steep') (Table 2; Fig. 5).

**Table 3** Slope gradient statistics for the different lithological units

Lithological class	Area (km <sup>2</sup> )	Min	Max	Mean	Std
Limestones–marbles	31.69	0.02	68.91	21.94	10.40
Neogene sediments	13.19	0.01	55.30	13.61	8.84
Schists and ophiolites	15.32	0.01	67.88	17.21	8.82
Loose quaternary deposits	5.10	0.01	64.65	12.82	11.30
Flysch	15.98	0.00	61.84	14.84	8.45

Note that as expected, ‘very steep’ slopes mostly occur on outcrops of massive limestone (Table 3). Such terrain is occasionally subject to rock falls and topples but these slopes are not usually subject to other types of failure. These areas are effectively eliminated in the model by the low rate assigned to this class in the lithology map.

### 3.2.7 Relative relief map

Relative relief is the difference between the highest and the lowest elevations in an area. This parameter affects the landslide manifestation as the high relief areas are usually occupied by the most cohesive formations (e.g., limestones) exposed in unfavorable climate conditions (e.g., intensive rainfalls). Within the limits of the study area, the relative relief ranges from 0 to 932 m. Furthermore, most of the higher relative relief values are found in areas occupied by limestones and schists-ophiolites classes (relatively stable formations), while the lowest values in areas occupied by Quaternary and Neogene sediments (erosion products).

### 3.2.8 Slope aspect map

Aspect can be defined as the slope direction, which identifies the downslope direction of the maximum rate of elevation change. Aspect is expressed in degrees from north and clockwise, ranging from 0 to 360. The value of 361° is used to identify flat surfaces such as water bodies.

The aspect of a slope can influence indirectly the landslide initiation, because it controls the exposition to several climate conditions (duration of sunlight exposition, precipitation intensity, moisture retention, etc.) and as a result the vegetation cover (Wieczorek et al. 1997; Dai et al. 2002; Cevik and Topal 2003; Suzen and Doyuran 2004; Komac 2006). In this study, the aspect map of the study area was classified into six classes; flat, SE, E and S, NE and SW, W and N, NW (Table 2). Based on hydrometeorological data of the study area, the NW oriented slopes are more violently affected by rainfalls.

### 3.2.9 Rainfall map

The hydrometeorological data for a time-period of 25 years, which collected and evaluated from the Power Plant Company of Greece, were used for the synthesis of the precipitation distribution map of Greece (IGME 1993). A digitized part of this map, referring to Rethymnon Prefecture, was incorporated to the data in order to include the high precipitation rates effect on the landslide hazard maps. High precipitation is characterized as the physical processes constituting the main triggering causal factors of landslides (WP/WLI 1994; Koukis et al. 1997; Polemio and Sdao 1999; Sdao and Simeone 2007). Within the limits of the study area, the average annual precipitation ranges from 800 to 1,400 mm. Three classes were defined, using an equal interval of 200 mm (Table 2).

## 4 Landslide hazard zonation maps

The different classes of thematic layers were assigned, the corresponding rating values as attribute information in the GIS and an ‘attribute map’ was generated for each data layer. The vector data layers were reclassified using the assigned rates and the related raster data

layers were produced. Finally, the reclassified raster layers were used as input parameters for the raster calculator function.

The landslide hazard zonation (LHZ) maps were produced within a raster/grid GIS. Raster models are cell-based representations of map features, which offer analytical capabilities for continuous data and allow fast processing of map layer overlay operations (Fig 5). In a raster GIS, the LHZ maps are calculated at a cell level using several approaches.

There are various approaches to the generation of landslide hazard maps. Examples can be found in Varnes (1984), Hartlen and Viberg (1988), van Westen (1994), Mantovani et al. (1996), and Mason and Rosenbaum (2002). Based on the available data, the WLC method (a semi-quantitative, logical elimination and characterization approach) has been applied since a detailed statistical assessment of the temporal and spatial distribution of landslides in the study area was difficult to be used.

The applied assessment model is based on the information provided by cartographic data, image data and survey materials, published literature, and field observation. The method can be broadly divided in three parts: (1) parameter (relevant to slope instability) selection and model configuration, (2) model implementation: thematic information extraction and multi-data layer generation, and (3) landslide hazard index computation and mapping. Using the nine raster thematic layers, three different models were applied. The three produced maps were smoothed using a  $3 \times 3$  low-pass filter in order to reduce the significance of possible anomalous cells. Moreover, the maps were normalized in order to be comparable quantities and then, they were classified using the equal interval method, in five classes: very low hazard, low hazard, moderate hazard, high hazard, and very high hazard.

#### 4.1 Simple landslide hazard index

The Landslide Hazard Index (LHI) for each grid cell is given by the summation of the raster thematic maps after their multiplication by the corresponding weights ( $W_1$  in Table 2). The LHI is presented by the expression as given below:

$$\text{LHI} = \sum_{i=1}^n \text{weight}_{w_1} \times \text{class rate} \quad (1)$$

where  $n$  is the total number of data layers.

#### 4.2 Lithology-based weighted landslide hazard index

Accordingly, in this map, the Landslide Hazard Index (LHI) for each grid cell is given by the summation of the raster thematic maps after their multiplication by the corresponding lithology-based weights ( $W_2$  in Table 2). The LHI is expressed as in the following equation:

$$\text{LHI}_L = \sum_{i=1}^n \text{weight}_{w_2} \times \text{class rate} \quad (2)$$

#### 4.3 Geometric mean based landslide hazard index

The Geometric Mean (GM) results to a multi-variable elimination in the model, which in turn is modified, in accordance with the data layer. The GM is a multiplication-based

approach that terminates whenever a zero value occurs and is therefore effective in masking off areas characterized by factors considered irrelevant (the most stable areas) to the phenomenon under investigation (Liu et al. 2004; Fourniadis et al. 2007). Through the use of 0 values, the geometric mean immediately eliminates the most stable areas from the assessment while it characterizes the areas which are particularly vulnerable to landslides.

The geometric mean is defined as below, (Fourniadis et al. 2007):

$$GM = \left( \prod_{i=1}^n \text{class rate} \right)^{1/n} \tag{3}$$

where, *n* is the total number of data layers.

The quantification system was mainly based on the information values of Table 2 with the following modifications; the rate 0 of the tectonic structures, streams, and roads layers was replaced by 1 as the great distance of them does not eliminate a landslide occurrence. On the contrary, the rate 1 was replaced by rate 0 in the data layer of slope, as it is considered to be critical for landslide events.

### 5 Data verification

The three produced normalized hazard maps were statistically processed in order to explore their correlation with each other. As it can be seen in Table 4 and Figs. 7, 8, and 9, there is a noticeable correlation between the simple weighted and the lithology-based weighted methods, while the less correlated maps are those derived from lithology-based weighted and geometric mean methods.

Furthermore, the validation of the above-presented maps was conducted by integrating them with the distribution of the landslides manifested in the study area until nowadays. The data concerning the landslides were coming from national databases (Koukis and Ziourkas 1991; Koukis et al. 1994, 1996, 1997) and from bibliographic sources (IGME records) covering a period of more than 45 years. Moreover, the above mentioned database

**Table 4** Comparison of the three normalized landslide hazard zonation maps

Layer	Min	Max	Mean	Std
Statistics of individual layers				
Lithology	0.1107	1	0.4277	0.1777
Geometric	0.0000	1	0.4751	0.2080
Simple	0.2764	1	0.6441	0.1020
Layer	Simple	Lithology	Geometric	
Covariance matrix				
Simple	8.19E-14	1.04E-13	9.28E-14	
Lithology	1.04E-13	2.39E-13	7.31E-14	
Geometric	9.28E-14	7.31E-14	3.29E-13	
Correlation matrix				
Simple	1	0.74152	0.56577	
Lithology	0.74152	1	0.26031	
Geometric	0.56577	0.26031	1	

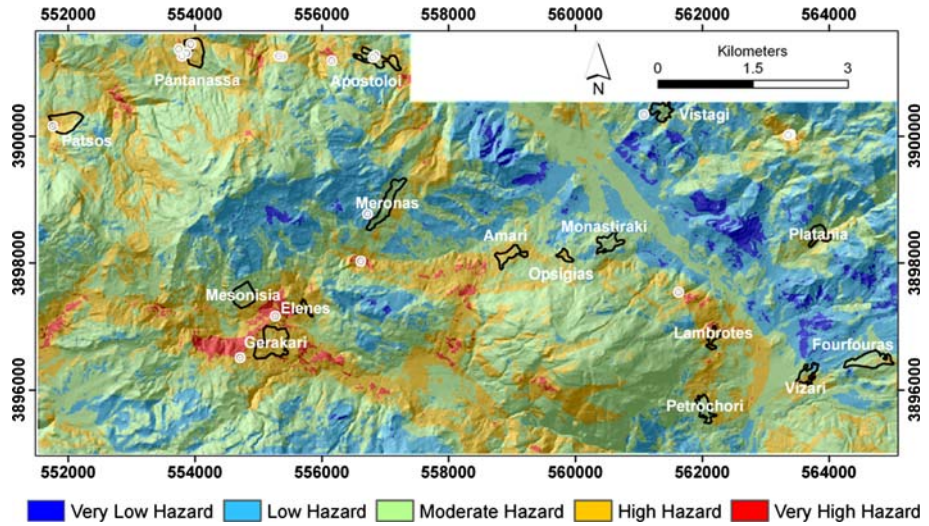


**Fig. 7** The simple Landslide Hazard Index for the study area

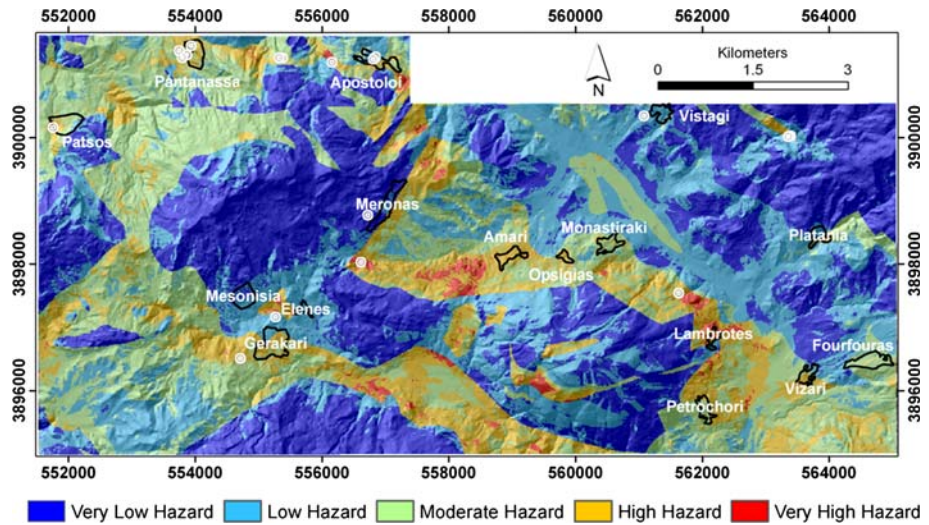


**Fig. 8** The lithology-based weighted derived Landslide Hazard Index for the study area

was enriched with data of new possible landslide locations which were mapped through image interpretation of the IKONOS satellite image. These possible landslides were checked through ground-truth in selected areas in order to verify the geological interpretation. Finally, these data were also used for the verification of the landslide hazard maps.

The image interpretation of the high-resolution satellite image pointed several locations as possible landslides but although it was expected that improved spatial resolution would lead to higher detection capability, the increase in spectral variance associated with higher resolution led in some cases to impaired spectral separability between landslides and other areas (Park and Chi 2007). Specifically, ground truth excluded two of a total of ten



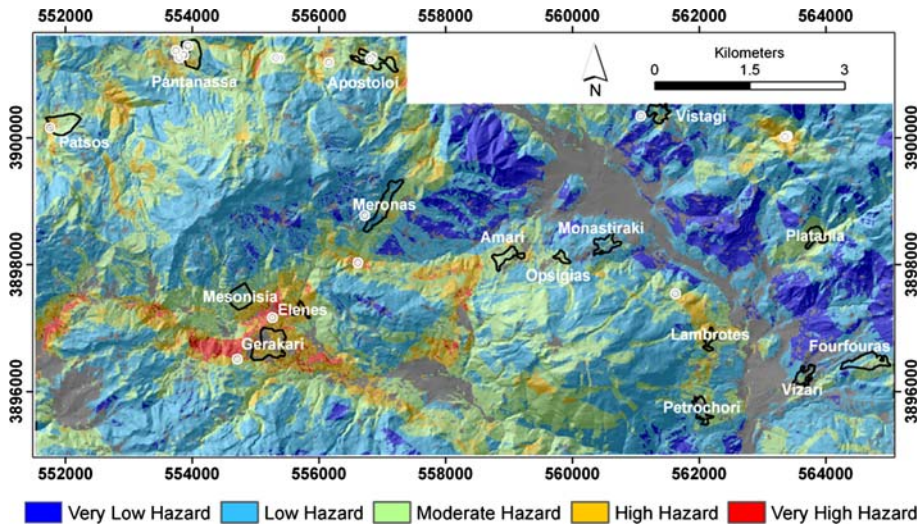


**Fig. 9** The Geometric Mean Landslide Hazard Index for the study area

locations, since some arable areas or quarries were initially considered as possible landslides (Fig. 10, location 1).

The exact locations of the manifested landslides are pointed in the hazard maps (Figs. 7, 8, 9) so that they could verify the hazardous areas.

### 6 Elements at landslide risk

In the study area, landslides affect people, buildings, transportation networks, and agricultural activities. Landslide risk can be estimated based on the following equation:

$$\text{Risk} = \text{hazard} \times \text{exposure} \tag{4}$$

The exposure factor was estimated by the combination of population density, land use, and road network data layers. The aforementioned data layers were classified and ranked according to the risk exposure of people, as shown in Table 5. Generally, larger values were assigned to population areas, built-up areas and road networks to reflect their higher significance in determining the impact of landslides.

The risk maps produced by that procedure wisely point the land occupied by the villages and by the arable-cultivated areas surrounding them as high to very high risk areas. Also, the areas in the proximity to the road network are characterized as moderate to high risk areas. All these areas are characterized by continuous human presence and they are related with economic activities. As an example, Fig. 11 presents the Risk map produced by using the simple LHI map.

### 7 Conclusions

The verification procedure proved that the produced landslide hazard and risk maps are substantial for land degradation management and planning of the study area. Although the

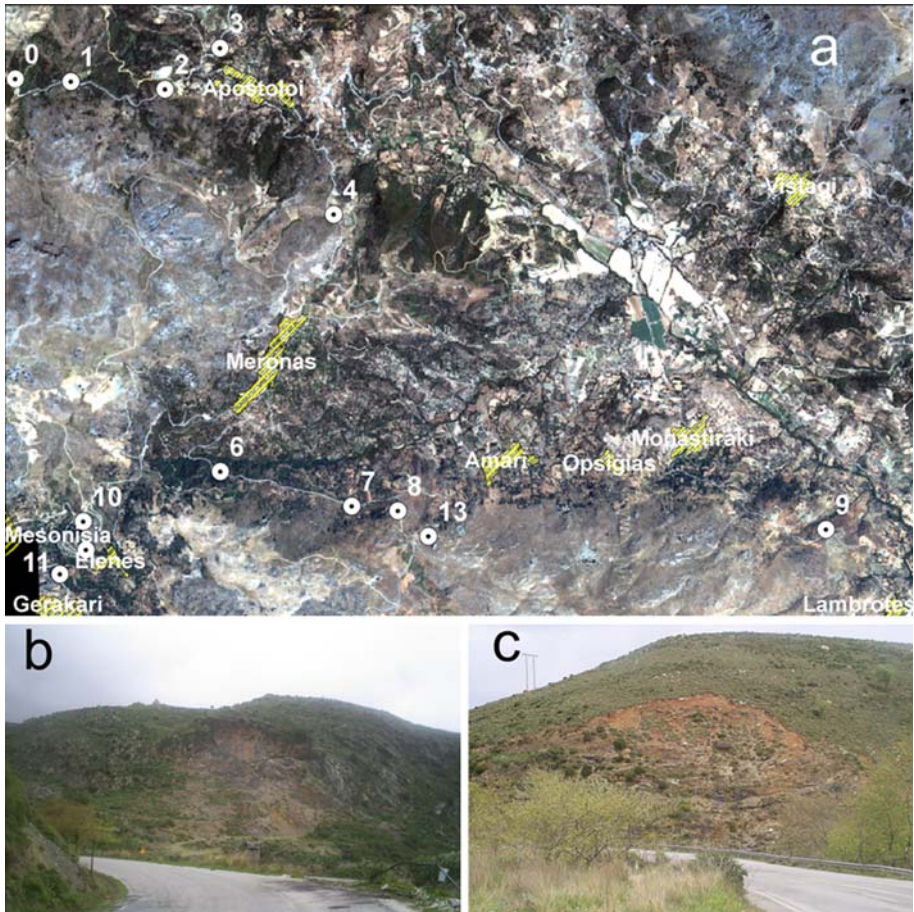


**Fig. 10** **a** 321 (R, G, B) Pan-sharpened IKONOS satellite image color composite with villages' vector layer overlaid. Possible landslide locations are depicted by *solid circles*. **b** Photo from *location 1* proving that the possible landslide was actually an abandoned quarry. **c** Photo from *location 6* verifying a landslide south to Merona village, occurred in the weathered mantle of Flysch formations. The preparatory causal factor of the landslide was the excavation along the toe of the slope during the road construction

WLC methodology results vary depending on the subjective knowledge of experts, in cases where the quality of the available data is high, and the weighting and rating factors are set correctly the results can be satisfactory.

As mentioned in the geological setting paragraph, the high hazard areas were expected to occur in areas which have the following characteristics; they should compose by landslide vulnerable geological formations (flysch, weathered mantle of the metamorphic rocks, Quaternary, and Neogene deposits) with extensive tectonic fragmentation, located on sections with intensive morphological relief, dense drainage and road network, and extensive human activities. Thus, the landslide hazard weighting-rating system was set accordingly in order to point the expected high hazard areas.

The verification procedure confirmed the accuracy of the indicated hazardous areas as well as the index setup procedure. As presented in the hazard maps, the majority of the

**Table 5** Vulnerability weighting-rating system adopted in this study

Elements at risk		Vulnerability	Rate	Weigh
Population density (km <sup>2</sup> )	Low	Moderate	3	10
	Moderate	High	6	
	High	Very high	9	
	Very high	Extremely high	10	
Land use	Urban areas	Extremely high	10	9
	Arable land (irrigated or non-irrigated)	High	8	
	Cultivated areas (vineyards, olive groves)	Moderate	5	
	Other areas	Low	2	
Road network	Distance to surfaced road ≤100 m	High	8	7
	Distance to unsurfaced road ≤50 m	Low	5	

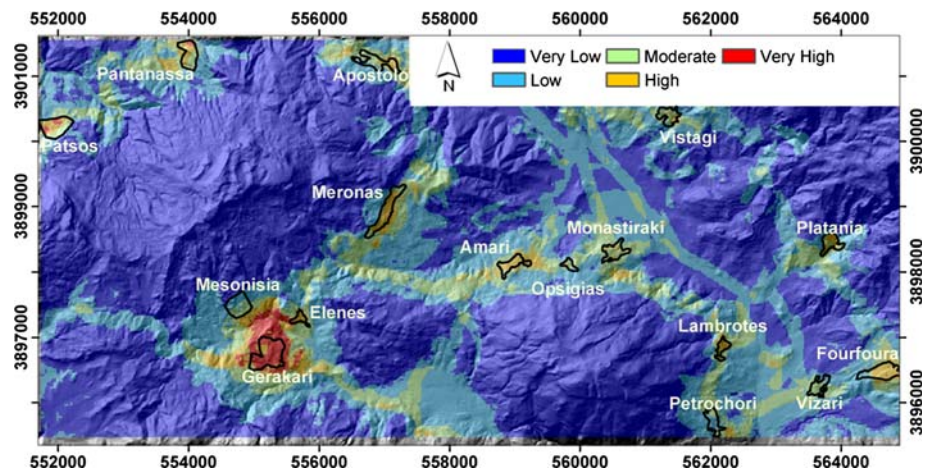


**Fig. 11** The Landslide Risk Map produced by using the Simple Landslide Hazard Map

activated and in many cases reactivated landslides is located in high or very high hazard areas (Figs. 7, 8, 9). These areas are occupied by landslide vulnerable geological formations.

It is proved that the integration of remote sensing and GIS techniques can support engineering geological studies concerning landslide vulnerability of small areas. Moreover, the great benefit of DEM is obvious as four out of the nine necessary layers for this study were produced using elevation data. Finally, this procedure can be helpful for the development of decision support systems and the continuous monitoring of areas prone to landslides.

**Acknowledgments** The project is co-funded by the European Social Fund and National Resources in the framework of the project INTERREG III B ARCHIMED, sub-project A1.020 entitled “Methodology integration of EO techniques as operative tool for land degradation management and planning in Mediterranean areas”. We are also grateful to the students (Nikos Nikakis and Argyro Stefanaki) involved in this work digitizing the topographic maps of the study area.

## References

- Aleotti P, Chowdhury R (1999) Landslide hazard assessment: summary review and new perspectives. *Bull Eng Geol Environ* 58:21–44. doi:[10.1007/s100640050066](https://doi.org/10.1007/s100640050066)
- Anbalagan D (1992) Landslide hazard evaluation and zonation mapping in mountainous terrain. *Eng Geol* 32:269–277. doi:[10.1016/0013-7952\(92\)90053-2](https://doi.org/10.1016/0013-7952(92)90053-2)
- Atkinson PM, Massari R (1998) Generalized linear modeling of landslide susceptibility in the central Apennines, Italy. *Comput Geosci* 24:373–385. doi:[10.1016/S0098-3004\(97\)00117-9](https://doi.org/10.1016/S0098-3004(97)00117-9)
- Ayalew L, Yamagishi H (2005) The application of GIS-based logistic regression for landslide susceptibility mapping in the Kakuda–Yahiko Mountains, Central Japan. *Geomorphology* 65:15–31. doi:[10.1016/j.geomorph.2004.06.010](https://doi.org/10.1016/j.geomorph.2004.06.010)
- Ayalew L, Yamagishi H, Ugawa N (2004a) Landslide susceptibility mapping using GIS-based weighted linear combination, the case in Tsugawa area of Agano River, Niigata Prefecture, Japan. *Landslides* 1: 73–81. doi:[10.1007/s10346-003-0006-9](https://doi.org/10.1007/s10346-003-0006-9)
- Ayalew L, Yamagishi H, Watanabe N, Marui H (2004b) Landslide susceptibility mapping using a semi-quantitative approach, a case study from Kakuda-Yahiko Mountains, Niigata, Japan. In: Free M, Aydin A (eds) Proceedings of the 4th asian symposium on engineering geology and the environment, Geological Society of Hong Kong, vol 7. pp 99–105
- Barredo JJ, Benavides A, Hervas J, van Westen CJ (2000) Comparing heuristic landslide hazard assessment techniques using GIS in the Tirajana basin, Gran Canaria Island, Spain. *Int J Appl Earth Obs Geoinf* 2:9–23. doi:[10.1016/S0303-2434\(00\)85022-9](https://doi.org/10.1016/S0303-2434(00)85022-9)
- Bonneau M (1973) Les différentes “séries ophiolitifères” de la Crète: une mise au point. *CR Acad Sci (D)* 276:1249–1252
- Brabb EE (1984) Innovative approaches to landslide hazard and risk mapping. In: Proceedings of the fourth international symposium on landslides, vol 1. Canadian Geotechnical Society, Toronto, pp 307–324
- Caniani D, Pascale S, Sdao F, Sole A (2008) Neural networks and landslide susceptibility: a case study of the urban area of Potenza. *Nat Hazards* 45:55–72. doi:[10.1007/s11069-007-9169-3](https://doi.org/10.1007/s11069-007-9169-3)
- Carrara A, Cardinali M, Guzzetti F, Reichenbach P (1995) GIS technology in mapping landslide hazard. In: Carrara A, Guzzetti F (eds) Geographical information systems in assessing natural hazard. Kluwer, London, pp 173–175
- Carrara A, Guzzetti F, Cardinali M, Reichenbach P (1999) Use of GIS technology in the prediction and monitoring of landslide hazard. *Nat Hazards* 20:117–135. doi:[10.1023/A:1008097111310](https://doi.org/10.1023/A:1008097111310)
- Castellanos Abella EA, van Westen CJ (2008) Qualitative landslide susceptibility assessment by multicriteria analysis: a case study from San Antonio del Sur, Guantánamo. *Cuba Geomorphol* 94(3–4):453–466
- Cevik E, Topal T (2003) GIS-based landslide susceptibility mapping for a problematic segment of the natural gas pipeline, Hendek (Turkey). *Environ Geol* 44(8):949–962. doi:[10.1007/s00254-003-0838-6](https://doi.org/10.1007/s00254-003-0838-6)
- Clerici A, Perego S, Tellini C, Vescovi P (2002) A procedure for landslide susceptibility zonation by the conditional analysis method. *Geomorphology* 48:349–364. doi:[10.1016/S0169-555X\(02\)00079-X](https://doi.org/10.1016/S0169-555X(02)00079-X)
- Creutzburg N (1977) General geological map of Greece (Crete Island). 1:200.000. IGRM, Athens
- Dai FC, Lee CF, Ngai YY (2002) Landslide risk assessment and management: an overview. *Eng Geol* 64(1):65–87. doi:[10.1016/S0013-7952\(01\)00093-X](https://doi.org/10.1016/S0013-7952(01)00093-X)
- De Roo APJ (1993) Modeling surface runoff and soil erosion in catchments using geographic information systems: validity and applicability of the “ANSWERS” model in two catchments in the loess area of South Limburg (The Netherlands) and one in Devon (UK). *Netherlands Geographical studies*, 157, University of Utrecht, Utrecht, p 304
- Dikau R, Cavallin A, Jager S (1996) Databases and GIS for landslide research in Europe. *Geomorphology* 15(3–4):227–239. doi:[10.1016/0169-555X\(95\)00072-D](https://doi.org/10.1016/0169-555X(95)00072-D)
- Ercanoglu M, Gokceoglu C (2004) Use of fuzzy relations to produce landslide susceptibility map of a landslide prone area (West Black Sea Region, Turkey). *Eng Geol* 75(3–4):229–250. doi:[10.1016/j.enggeo.2004.06.001](https://doi.org/10.1016/j.enggeo.2004.06.001)
- Evans NC, Huang SW, King JP (1997) The natural terrain landslide study—phases I and II. Special project report SPR5/97, Geotechnical Engineering Office, Hong Kong
- Fall M (2000) Standsicherheitsanalyse der Küstenhänge in Cap Manuel (Dakar, Senegal) mit Hilfe ingenieurgeologisch-geotechnischer Untersuchungen und GIS-technologischer Methoden, vol 2000–2002. Veröffentlichung Institut Geotechnik, Heft, p 187
- Fall M, Azzam R (2001a) Ingenieurgeologische und numerische Standsicherheitsanalysen der Basaltkliffe in Dakar. *Int J Felsbau* 19(1):51–57
- Fall M, Azzam R (2001b) An example of multi-disciplinary approach to landslide assessment in coastal area. International conference on landslide, proceedings international conference on landslides: causes impacts and countermeasures, Glückauf Verlag, Davos, pp 45–54

- Fall M, Dia A, Fall M, Gbaguidi I, Lo PG, Diop IN (1996) Un cas d'instabilité de pente naturelle: le versant des Madeleines—Presqu'île de Dakar (Sénégal): analyse, Cartographie des risques et prévention. *Bull Eng Geol Environ* 53:29–38. doi:[10.1007/BF02594938](https://doi.org/10.1007/BF02594938)
- Fall M, Azam R, Noubactep C (2006) A multi-method approach to study the stability of natural slopes and landslide susceptibility mapping. *Eng Geol* 82(4):241–263. doi:[10.1016/j.enggeo.2005.11.007](https://doi.org/10.1016/j.enggeo.2005.11.007)
- Fell R, Walker B, Finlay P (1996) Estimating the probability of landsliding. In: Proceedings of the 7th Australia–New Zealand conference on geomechanics, Institute of Engineers, Adelaide, pp 304–311
- Fitroulakis N (1980) The geological structure of Crete Island. Problems—observations—conclusions. PhD thesis, Technical University of Athens, Athens
- Fourniadis IG, Liu JG, Mason PJ (2007) Landslide hazard assessment in the three gorges area, China, using ASTER imagery: Wushan–Badong. *Geomorphology* 84:126–144. doi:[10.1016/j.geomorph.2006.07.020](https://doi.org/10.1016/j.geomorph.2006.07.020)
- Gray DH, Leiser AT (1982) Biotechnical slope protection and erosion control. Van Nostrand Reinhold, New York
- Greenway DR (1987) Vegetation and slope stability. In: Anderson MG, Richards KS (eds) *Slope stability*. Wiley, New York, pp 187–230
- Guzetti F, Carrara A, Cardinali M, Reichenbach P (1999) Landslide hazard evaluation: a review of current techniques and their application in a multiscale study, Central Italy. *Geomorphology* 31:181–216. doi:[10.1016/S0169-555X\(99\)00078-1](https://doi.org/10.1016/S0169-555X(99)00078-1)
- Hartlen J, Viberg L (1988) General report: evaluation of landslide hazard. In: Proceedings of the fifth international symposium on landslides, Balkema, Lausanne, pp 1037–1057
- Huang R, Li Y (1992) Logical model of slope stability prediction in the three gorges reservoir area, China. In: Proceedings of the sixth international symposium on landslides—Glissements de terrain, Balkema, Christchurch, pp 977–981
- Hutchinson J, Chandler M (1991) A preliminary landslide hazard zonation of the undercliff of the Isle of Wight. In: Chandler R (ed) *Slope stability engineering. Developments and applications*. Thomas Telford, London, pp 197–206
- Institute of Geology and Mineral Exploration—IGME (1985) Geological map of Greece—Melambes sheet (scale 1:50.000). IGME, Athens
- Institute of Geology and Mineral Exploration—IGME (1991) Geological map of Greece—Perama sheet (Scale 1:50.000). IGME, Athens
- Institute of Geology and Mineral Exploration—IGME (1993) Geological map of Greece (Scale 1:500.000). IGME, Athens
- Komac M (2006) A landslide susceptibility model using the analytical hierarchy process method and multivariate statistics in perialpine Slovenia. *Geomorphology* 74(1–4):17–28. doi:[10.1016/j.geomorph.2005.07.005](https://doi.org/10.1016/j.geomorph.2005.07.005)
- Koukis G, Ziourkas C (1991) Slope instability phenomena in Greece: a statistical analysis. *Bull IAEG* 43: 47–60
- Koukis G, Tsiambaos G, Sabatakakis N (1994) Slope movements in the Greek territory: a statistical approach. In: Proceedings of 7th international IAEG congress, Balkema, Rotterdam, pp 4621–4628
- Koukis G, Tsiambaos G, Sabatakakis N (1996) Landslides in Greece: research evolution and quantitative analysis. In: Senneset K (ed) *Proceedings of 7th international symposium on landslides*, Balkema, Rotterdam, pp 1935–1940
- Koukis G, Tsiambaos G, Sabatakakis N (1997) Landslide movements in Greece: engineering geological characteristics and environmental consequences. In: Proceedings of international symposium of engineering, geology and the envnar, IAEG, Balkema, Rotterdam, pp 789–792
- Koukis G, Sabatakakis N, Nikolaou N, Loupasakis C (2005) Landslide hazard zonation in Greece. In: Sassa K, Fukuoka H, Wang F, Wang G (eds) *Proceedings of open symposium on landslide risk analysis and sustainable disaster management in the First General Assembly of International Consortium on Landslides*, Springer-Verlag, Berlin, pp 291–296
- Lee EM, Jones DKC (2004) *Landslide risk assessment*. Thomas Telford, London, p 454
- Lee S, Choi J, Min K (2004a) Probabilistic landslide hazard mapping using GIS and remote sensing data at Boun, Korea. *Int J Remote Sens* 25(11):2037–2052. doi:[10.1080/01431160310001618734](https://doi.org/10.1080/01431160310001618734)
- Lee S, Ryu J, Won J, Park H (2004b) Determination and application of the weight for landslide susceptibility mapping using an artificial neural network. *Eng Geol* 71:289–302. doi:[10.1016/S0013-7952\(03\)00142-X](https://doi.org/10.1016/S0013-7952(03)00142-X)
- Leroi E (1997) Landslide risk mapping: problems, limitation and developments. In: Cruden Fell (ed) *Landslide risk assessment*. Balkema, Rotterdam, pp 239–250
- Liu JG, Mason PJ, Clerici N, Chen S, Davis A, Miao F, Deng H, Liang L (2004) Landslide hazard assessment in the three gorges area of the Yangtze river using ASTER imagery: Zigui–Badong. *Geomorphology* 61(1–2):171–187. doi:[10.1016/j.geomorph.2003.12.004](https://doi.org/10.1016/j.geomorph.2003.12.004)

- Luzi L, Pergalani F, Terlien MTJ (2000) Slope vulnerability to earthquakes at subregional scale, using probabilistic techniques and geographic information systems. *Eng Geol* 58(3–4):313–336. doi:[10.1016/S0013-7952\(00\)00041-7](https://doi.org/10.1016/S0013-7952(00)00041-7)
- Mantovani F, Soeters R, van Westen CJ (1996) Remote sensing techniques for landslide studies and hazard zonation in Europe. *Geomorphology* 15:213–225. doi:[10.1016/0169-555X\(95\)00071-C](https://doi.org/10.1016/0169-555X(95)00071-C)
- Mason PJ, Rosenbaum MS (2002) Predicting future landslides in a residential area on the basis of geohazard mapping: the Langhe Hills in Piemonte, NW Italy. *Q J Eng Geol Hydrol* 35:317–326. doi:[10.1144/1470-9236/00047](https://doi.org/10.1144/1470-9236/00047)
- Miles SB, Ho CL (1999) Rigorous landslide hazard zonation using Newmark's method and stochastic ground motion simulation. *Soil Dyn Earthquake Eng* 18(4):305–323. doi:[10.1016/S0267-7261\(98\)00048-7](https://doi.org/10.1016/S0267-7261(98)00048-7)
- Miles SB, Keefer DK (1999) Evaluation of seismic slope-performance models using a regional case study. *Environ Eng Geosci* 6(1):25–39. doi:[10.1046/j.1526-0984.1999.08023.x](https://doi.org/10.1046/j.1526-0984.1999.08023.x)
- Montgomery DR, Schmidt KM, Dietrich WE, Greenberg HM (2000) Forest clearing and regional landslide in the Pacific Northwest. *Geology* 28:311–314. doi:[10.1130/0091-7613\(2000\)28<311:FCA RL>2.0.CO;2](https://doi.org/10.1130/0091-7613(2000)28<311:FCA RL>2.0.CO;2)
- Moon A, Olds R, Wilson R, Burman B (1992) Debris flow zoning at Montrose, Victoria. In: Proceedings of 6th international symposium on landslides, vol 2. Balkema, Rotterdam, pp 1015–1022
- Nash D (1987) A comparative review of limit equilibrium methods of slope stability analysis. In: Anderson MG, Richards KJ (eds) *Slope stability*. Wiley, New York, pp 11–75
- Park NW, Chi KH (2007) Quantitative assessment of landslide susceptibility using high-resolution remote sensing data and a generalized additive model'. *Int J Remote Sens* 29(1):247–264. doi:[10.1080/01431160701227661](https://doi.org/10.1080/01431160701227661)
- Polemio M, Sdao F (1999) The role of rainfall in the landslide hazard: the case of the Avigliano urban area (southern Apennines, Italy). *Eng Geol* 53(3–4):297–309. doi:[10.1016/S0013-7952\(98\)00083-0](https://doi.org/10.1016/S0013-7952(98)00083-0)
- Refice A, Capolongo D (2002) Probabilistic modeling of uncertainties in earthquake-induced landslide hazard assessment. *Comput Geosci* 28(6):735–749. doi:[10.1016/S0098-3004\(01\)00104-2](https://doi.org/10.1016/S0098-3004(01)00104-2)
- Saaty TL (1980) *The analytical hierarchy process*. McGraw Hill, New York
- Saha AK, Gupta RP, Arora MK (2002) GIS-based landslide hazard zonation in the Bhagirathi (Ganga) valley, Himalayas. *Int J Remote Sens* 23(2):357–369. doi:[10.1080/01431160010014260](https://doi.org/10.1080/01431160010014260)
- Sdao F, Simeone V (2007) Mass movements affecting Goddess Mefitis sanctuary in Rossano di Vaglio (Basilicata, southern Italy). *J Cult Herit* 8(1):77–80
- Siddle HJ, Jones DB, Payne HR (1991) Development of a methodology for landslip potential mapping in the Rhondda valley. In: Chandler RJ (ed) *Slope stability engineering*. Thomas Telford, London, pp 137–142
- Soeters R, van Westen CJ (1996) Slope instability recognition, analysis, and zonation. In: Turner KA, Schuster RL (eds) *Landslides: investigation and mitigation*. Transport Research Board Special Report, vol 247. pp 129–177
- Strahler AN (1957) Quantitative analysis of watershed geomorphology. *Trans Am Geophys Union* 38:913–920
- Strahler AN (1964) Quantitative geomorphology of basins and channel networks. In: Chow VT (ed) *Handbook of applied hydrology*. McGraw Hill, New York
- Suzen ML, Doyuran V (2004) Data driven bivariate landslide susceptibility assessment using geographical information systems: a method and application to Asarsuyu catchment, Turkey. *Eng Geol* 71:303–321. doi:[10.1016/S0013-7952\(03\)00143-1](https://doi.org/10.1016/S0013-7952(03)00143-1)
- Tataris A, Christodoulou C (1965) The geological structure of Leuca Mountains. *Bull Geol Soc Greece* 6:319–347
- Terlien MTJ, Van Asch ThWJ, van Westen CJ (1995) Deterministic modelling in GIS-based landslide hazard assessment. In: Carrar A, Guzzetti F (eds) *Geographical information systems in assessing natural hazards*. Kluwer, London, pp 57–77
- Tsiampaos G (1989) Engineering geological characteristics of the Iraklion marls, Crete, PhD Thesis, Technical Chamber of Greece, Iraklion, p 358
- van Westen CJ (1994) GIS in landslide hazard zonation: a review, with examples from the Andes of Colombia. In: Price M, Heywood I (eds) *Mountain environments and geographic information system*. Taylor and Francis, London, pp 135–165
- van Westen CJ, Rengers N, Terlien MTJ (1997) Prediction of the occurrence of slope instability phenomena through GIS-based hazard zonation. *Geol Rundsch* 86:4004–4414
- Varnes DJ (1978) Slope movement types and processes. In: Schuster RL, Krizek RJ (eds) *Landslides: analysis and control*, special report 176. Transportation Research Board, National Academy of Sciences, Washington, pp 11–33
- Varnes DJ, IAEG Commission on landslides and other mass-movements (1984) *Landslide hazard zonation: a review of principles and practice*. UNESCO Press, Paris

- Ward TJ, Li RM, Simons DB (1981) Use of a mathematical model for estimating potential landslide sites in steep forested drainage basins. *IAHS Publ* 132:21–41
- Wieczorek GF, Mandrone G, DeCola L (1997) The influence of hillslope shape on debris-flow initiation. In: Chen CL (ed) *Debrisflow hazards mitigation: mechanics, prediction, and assessment*. American Society of Civil Engineers, New York, pp 21–31
- WP/WLI (International Geotechnical Societies' UNESCO Working Party on World Landslide Inventory) (1994) A suggested method for reporting landslides causes. *Bull Int Assoc Eng Geol* 50:71–74. doi: [10.1007/BF02594958](https://doi.org/10.1007/BF02594958)
- Wu S, Shi L, Wang R, Tan C, Hu D, Mei Y, Xu R (2001) Zonation of the landslide hazard in the fore-reservoir region of the three gorges project on the Yangtze River. *Eng Geol* 59:51–58. doi: [10.1016/S0013-7952\(00\)00061-2](https://doi.org/10.1016/S0013-7952(00)00061-2)
- Yalcin A (2008) GIS-based landslide susceptibility mapping using analytical hierarchy process and bivariate statistics in Ardesen (Turkey): comparisons of results and confirmations. *Catena* 72:1–12. doi: [10.1016/j.catena.2007.01.003](https://doi.org/10.1016/j.catena.2007.01.003)